Lineage and Spatial Mapping of Glioblastoma-associated Immunity

Vidhya M. Ravi[1,2,3,4,#], Nicolas Neidert[1,2,3,#], Paulina Will[1,2,3], Kevin Joseph[1,2,3], Julian P. Maier[1,2,3], Jan Kückelhaus[1,2,3], Lea Vollmer[1,2,3], Jonathan M Goeldner[1,2,3], Simon P. Behringer[1,2,3], Florian Scherer[3,5], Melanie Boerries[3,6,7,8], Marie Follo[3,5], Tobias Weiss[9], Daniel Delev[10,11], Julius Kernbach[10,11], Pamela Franco[3,4], Nils Schallner[3,12], Christian Scheiwe[2,3], Maria Stella Carro[3,4], Ulrich G. Hofmann[3,4], Christian Fung[2,3], Jürgen Beck[2,3,15], Roman Sankowski[3],[13], Marco Prinz[3,13,14,15], **Oliver Schnell[2,3,16,†], Dieter Henrik Heiland[1,2,3 †]**

[1]*Microenvironment and Immunology Research Laboratory, Medical* Center*, University of Freiburg, Germany*

[2]*Department of Neurosurgery, Medical Center, University of Freiburg, Germany*

[3]*Faculty of Medicine, Freiburg University, Germany*

[4]*Neuroelectronic Systems, Medical Center, University of Freiburg, Germany*

[5]*Department of Medicine I, Medical Center – University of Freiburg, Faculty of Medicine, University of Freiburg, Germany.*

[6]*Institute of Medical Bioinformatics and Systems Medicine, Medical Center-University of Freiburg, 79110 Freiburg, Germany.*

[7]*Comprehensive Cancer Center Freiburg (CCCF), Faculty of Medicine and Medical Center - University of Freiburg, 79106 Freiburg, Germany.*

[8]*German Cancer Consortium (DKTK), partner site Freiburg.*

[9]*Department of Neurology and Brain Tumor Center, University Hospital Zurich and University of Zurich, Switzerland*

[10]*Department of Neurosurgery, RWTH University of Aachen, Aachen, Germany*

[11] *Neurosurgical Artificial Intelligence Laboratory Aachen (NAILA), Department of Neurosurgery, RWTH University of Aachen, Aachen, Germany*

[12]*Department of Anesthesiology and Critical Care Medicine, Medical Center-University of Freiburg, 79106 Freiburg, Germany*

[13]*Institute of Neuropathology, Medical Center - University of Freiburg,*

[14]*Signalling Research Centres BIOSS and CIBSS, University of Freiburg, Germany*

[15]*Center for NeuroModulation (NeuroModul), University of Freiburg, Freiburg, Germany*

[16]Translational *NeuroOncology Research Group, Medical* Center*, University of Freiburg, Germany*

 # Equal contributed first authorship

† Equal contributed last authorship

DISCLOSURE OF CONFLICTS OF INTEREST: No potential conflicts of interest were disclosed by the authors.

Corresponding author:

Dieter Henrik Heiland

Department of Neurosurgery

Medical Center University of Freiburg

Breisacher Straße 64

79106 Freiburg

-Germany-

Tel: +49 (0) 761 270 50010

Fax: +49 (0) 761 270 51020

E-mail: dieter.henrik.heiland@uniklinik-freiburg.de

Highlights:

- Lineage tracking of T cells reveal IL10 driven exhaustion in glioblastoma
- *In-silico* modeling of spatial- and scRNA-sequencing identified a subset of *HMOX1*$^{+}$ myeloid cells releasing IL10.
- T cell exhaustion is spatially enriched in mesenchymal-like tumor regions.
- Human neocortical sections with autograft T cell stimulation confirmed IL10 dependent T cell exhaustion in mesenchymal-like tumors.

Visual Abstract:

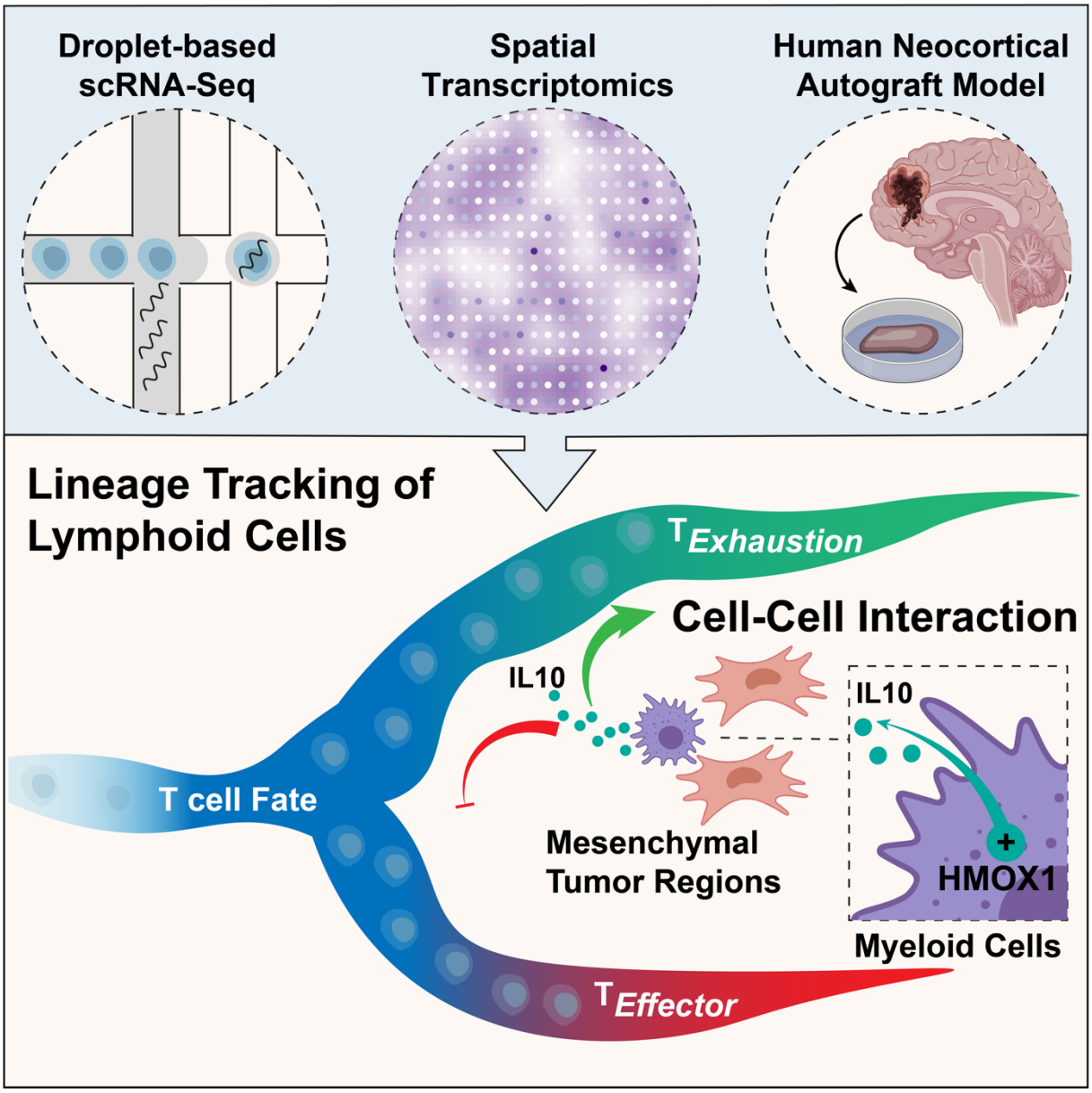

Abstract

The diversity of molecular states and cellular plasticity of immune cells within the glioblastoma environment remain poorly investigated. Here, we performed scRNA-sequencing of the immune compartment, mapping potential cellular interactions that lead to the exhausted phenotype of T cells. We identified Interleukin 10 response during T cell activation leading to the exhausted state. By use of an *in-silico* model, we explored cell-cell interactions and identified a subset of myeloid cells defined by high expression of *HMOX1* driving T cell exhaustion. We showed a spatial correlation between T cell exhaustion and mesenchymal-like gene expression, co-located with *HMOX1* expressing myeloid cells. Using human neocortical sections with myeloid cell depletion, we confirmed the functional interaction of myeloid and lymphoid cells, leading to the exhausted state of T cells. A comprehensive understanding of cellular states and plasticity of lymphoid cells in GBM aids in providing successful immunotherapeutic approaches.

Introduction

Tumor infiltrating lymphocytes along with brain resident and migrated myeloid cells on the other side, account for a meaningful part of tumor microenvironment in glioblastoma[1–3]. Most recently, the characterization of the myeloid cell population using scRNA-sequencing revealed a remarkable heterogeneity regarding cellular diversity and plasticity within the myeloid compartment[1,4]. Rather, the diversity of lymphoid cell types in malignant brain tumors has been poorly explored, although gaining insights into the heterogeneity of cell type composition and properties of gene expression will aid in providing successful approaches for immune therapy in the future. In other cancer entities such as colorectal cancer[5], liver cancer[6] or melanoma[7], different states of T cells have been investigated. Prolonged immune activation and ambiguous stimulation, such as uncontrolled tumor growth or chronic infections, reduces the ability of $CD8^+$ lymphocytes to secrete proinflammatory cytokines and maintain their cytotoxic activity[7–9]. This cellular state, named dysfunctional or "exhausted" $CD8^+$ lymphocytes, represents a paramount barrier to successful vaccination or checkpoint therapy[2,10,11]. T cell exhaustion is partially orchestrated by regulation via inhibitory cell surface receptors (PD-1, CTLA-4, LAG-3, TIM-3 and others) and anti-inflammatory cytokines such as IL-10 and TGF-beta. Glioblastoma, a common and very aggressive primary brain tumor in adults, is archetypical for tumors with a strong immunosuppressive microenviroment[12] and current immunotherapeutic approaches such as PDL1/PD1 checkpoint blockade[13] or peptide vaccination[14], which led to remarkable responses in several cancers, failed to demonstrate activity in patients with glioblastoma.

To address the limited knowledge of lymphoid cell population in glioblastoma, we performed deep transcriptional profiling by scRNA-sequencing, mapped potential cellular interactions and cytokine responses that could lead to the dysfunctional and exhausted phenotype of T cells. Pseudotime analysis revealed increased Interleukin 10 (IL10) response during the transformation from the effector to the exhausted state in T cells. To computationally explore connected cells driving this transformation, we introduced a novel approach termed "*nearest functionally connected neighbor* (NFCN)", which identified a subset of myeloid cells marked by *CD163*$^+$ and *HMOX1*$^+$ expression. Furthermore, we applied spatial transcriptomics, which confirmed a spatial overlap of exhausted T cells with *HMOX1*$^+$ myeloid cells within mesenchymal enriched regions. Further, using a human neocortical slice model with myeloid cell depletion and T cell stimulation, we validated our findings from the computational approach, which depicts the role of myeloid cells as drivers of T cell exhaustion.

Results:

scRNA-Seq Charts the Immune Cell Compartment in Glioblastoma

In order to interrogate the diversity of the immune microenvironment in untreated glioblastomas, we profiled freshly obtained tumor specimens from 4 glioblastoma patients at first diagnosis using 3'-scRNA-seq (droplet-based 10X Genomics). To focus on the immune environment, in particular the heterogeneity of T cells, we sorted cells for the pan T cell marker $CD3^+$, **Figure 1a and Supplementary Figure 1a**. The scRNA-seq data consisted of 17,705 cells, with a median number of 2,022 unique molecular identifiers (UMIs) and approximately 897 uniquely expressed genes per cell. We corrected the data for the percentage of mitochondrial genes and removed batch effects due to technical artifacts. Next, we decomposed eigenvalue frequencies of the first 100 principal components and determined the number of non-trivial components by comparing them to randomized expression values, resulting in 35 meaningful components. Shared nearest neighbor (SNN) graph clustering resulted in 17 clusters containing significantly uniquely expressed genes, **Supplementary Figure 1b-c**. The major observed cell type when using the semi-supervised subtyping algorithm of scRNA-seq (SCINA-Model)[15] and SingleR[16] are microglia cells (*TMEM119, CX3CR1* and *P2RY12*) and macrophages (*AIF1, CD68, CD163* and low expression of *TMEM119, CX3CR1*), followed by $CD8^+$ T cells (*CD8A, CD3D*), natural killer cells (*KLRD1, GZMH, GZMA, NKG7* and *CD52*), $CD4^+$ T cells (*BCL6, CD3D, CD4, CD84* and *IL6R*), T-memory cells (*TRBC2, LCK, L7R* and *SELL*), granulocytes (*LYZ*), a minor amount of oligodendrocytes and oligodendrocyte-progenitor cell (OPC's) (*OLIG1, MBP, PDGFA*), and endothelia cells (*CD34, PCAM1, VEGFA*) **Figure 1b and Supplementary Figure 1c-g**. Furthermore, we inferred largescale copy number variations (CNVs) from scRNA-seq profiles by averaging expression over stretches of 100 genes on their respective chromosomes[17]. We confirm that there was only a very low level of contaminating tumor cells present (clustered as OPC cells), based on their typical chromosomal alterations (gain in chromosome 7 and loss in chromosome 10), **Supplementary Figure 2.**

Diversity of T cells in the Glioblastoma Microenvironment

To investigate the diversity of T cells in the microenvironment, we examined them by two different but complementary methods. First, in-silico the T cells were isolated by clustering (as shown above), based on their published marker gene expression profile ($CD3^+$, $CD4^+$/$CD8^+$). Secondly, they were isolated using the SCINA model, which result in a total number of 2,891 cells (detailed description in the method part), **Figure 1c**. To focus on the different regulatory states of these cells, we identified five subgroups

using SNN-clustering as well as pseudotime trajectories (STREAM[18]), closely reflecting the different activation states as recently described[8], **Figure 1c and Supplementary Figure 3a**. Pseudotime analysis is a computational approach by reconstructing lineage differentiation trajectories, which provide insights into transformation of cells over time and map fate decisions[18]. Cluster 1 contains cells marked by the expression of *CCL5* and *NKG7* and is enriched with the signature of naive T cells[8] (resting T cells), **Supplementary Figure 3a-b**, whereas the signature genes of activated T cells was enriched in cluster 2 (*GNLY, TNFAIP3, GZMB*), **Supplementary Figure 3 a-b.** Clusters 3 and 4 contain high expression of known exhaustion markers such as *HAVCR2*, CYBB and *VSIR,* and are highly enriched for the T cell exhaustion signature, **Figure 1d and Supplementary Figure 3 a-b.** However, cluster 3 revealed strong expression of proliferation markers such as *TOP2A* and *MKI67*, and enriched for the proliferation signature (GSEA), **Figure 1e**, and uniquely expressed markers of the dysfunctional activated state, suggesting that these cells represent an intermediate state between T effector cells and fully exhausted T cells. Based on our findings, we define cluster 1 as naive T cells (*SELL*, *CCR7* and *IL7R*) with enriched WNT signaling, cluster 2 represents T effector cells (*CD28*, *ICOS* and *IL2RB*) and showed IL2/IL12 pathway enrichment. The exhaustion clusters (cluster 3 and 4) were highlighted by a subset of exhaustion markers, **Figure 1d**, although classical markers such as *CTLA4* or *PDCD1* are lacking, **Supplementary Figure 3c**.

Dysfunctional State of T cells Driven by IL-10 Signaling

To gain insights into the regulatory mechanism involved, we reconstructed fate decisions made during T cell exhaustion using pseudotime trajectories. We identified 3 branches and 4 states in the present dataset in which T cells can exist, ranging from effector T cells to dysfunctional activation and exhaustion, **Figure 1c,f**. In the following section, SNN-clustering of T cells will be referred to as C1-5 and pseudo-timepoints as S0-3. We noticed that in both effector T cells (S3) as well as in dysfunctional activated and exhausted T cells, that proliferation markers remained upregulated (*TOP2A, MKI67*), **Figure 1g**. Additionally, we observed an increase in the Interleukin 10 (IL10) and INF-gamma response, **Figure 1h**, while *IFNG* expression was found exclusively in effector T cells (S3), **Supplementary Figure 3d.** In addition, we arranged all cells along the trajectory from S3 (effector T cells) over the states: from S0 (naive), S1 (T cell activation) to S2 (exhausted T cells), and mapped signature genes from T cell activation and exhaustion, **Figure 1i**, as well as pathway enrichments (**Figure 1i top**) of the IL-10 and IFN-gamma pathway. Leaf genes of the S3 branch were more likely mapped to T cell activation, whereas

leaf genes of S2 were more likely to be classified as exhausted genes. We also showed that genes of the IL-10 signature belonged to the set of transient genes that remained increased during the activation process of T cells as well in the exhausted state, **Figure 1i**. In summary, our data suggested that response to IL-10 and IFN-gamma contributed to the dysfunctional state of T cells and affected fate decisions. To gain insights into accurate downstream signaling of IL-10, IFN-gamma, as well as IL2, we created a library of the 50 most highly up- and downregulated genes, **Figure 2a-b**. Next, we extracted signatures observed in the different T cell clusters and compared them with the stimulation T cells. As expected, IL2 upregulated genes were significantly enriched in clusters 1 and 2, while IFN gamma and IL-10 marker genes showed a significant enrichment in the dysfunctional clusters 3 and 4, **Figure 2c.** Furthermore, we mapped signature genes from T cell clusters 1-4 along the different stimulations, **Figure 2d**. In agreement with our assumed conclusions a large subset of exhausted genes was highly enriched in T cells stimulated with IL-10 alone or in combination with IFN-gamma (*CYBB, HAVCR2, LAG3, VSIR, CTLA4*). Stimulation with IL2 caused increased activation marked by *GNLY, NKG7, IL2RB*.

A Subset of Microglia and Macrophages Drive IL-10 Stimulation

In our recent investigation[19], the crosstalk between reactive astrocytes of the tumor microenvironment and microglia cells was found to be responsible for upregulating IL10 release through microglia/macrophages caused by stimulation with IFN gamma and leading to JAK/STAT activation in tumor-associated astrocytes. In this study we introduce the “nearest functionally connected neighbor” algorithm, an in-silico model to identify the most likely related cell pairs through divergent down- and up-stream signal activity, **Figure 3a**. In our model, we assume that cellular interaction with distinct mutual activation implies two fundamental prerequisites. On the one hand the ligand needs to be expressed and released, or otherwise exposed on the cell surface. To avoid the chances of randomly elevated expression or technical artifacts, we also looked at simultaneous occurrence of ligand induction (upstream pathway signaling). On the other hand, the receptor needs to be expressed, and the downstream signaling has to be activated as well. This allows predicting the functional status of the receiver cell (Explanation of the model can be found in the methods section, with an overview in the **Figure 3a**).

We used our in-silico-model to screen for potential cells responsible for IL-10 activation of T cells. The algorithm identified pairs of lymphoid (T cell clusters) and myeloid cells (macrophages and microglia cluster) and estimated the likelihood of mutual activation, **Figure 3b**. By extraction of nearest connected

198 cells (top 10% ranked cells), we identified a subset of myeloid cells marked by remarkably high *IL10*
199 expression, **Figure 3b.** Within the receiver cells most of the connected cells (top 10% ranked cells)
200 originated from the exhausted T cell clusters 3 and 4, **Figure 3c-d.** The ligand cells that release IL10
201 (ligand-cells) on the other hand were located in the myeloid clusters (clusters 4 and 5, according to the
202 initial SNN-clustering containing the whole dataset), **Supplementary Figure 1**, and predominantly
203 expressed the markers of activated myeloid cells (*CD163*, *CD68*), as well as recently described marker
204 genes for glioma-associated microglia (GAM)[4] cells (*VEGFA* and *SPP1),* **Supplementary Figure 4**. The
205 highly connected ligand cells showed little to no expression of the inflammatory genes *IL1B* or *IL6*,
206 **Supplementary Figure 4**. In order to explore the difference between connected and non-connected
207 cells we examined in-silico extract connected and non-connected cells, which were defined by the
208 highest and lowest interaction-scores (quantile 97.5%). Using differential gene expression analysis we
209 observed multiple genes which confirmed the non-inflammatory polarization status of highly connected
210 cells. These findings are not surprising, since one of the essential markers of non-inflammatory myeloid
211 cells is *IL10*. We showed that the subset of most highly connected cells, marked by $CD168^{+}$ - $VEGFA^{+}$
212 - $IL1B^{-}$ - $IL6^{-}$ express increased levels of heme oxygenase 1 (*HMOX1)*. *HMOX1* is activated during
213 inflammation and oxidative injuries and is regulated through the Nrf2/Bach1-axis, as well as through the
214 IL10/HO1-axis. This gene is also well known to be upregulated in alternative activated macrophages[20].
215 Consistent with our findings, most downstream signals of the IL10/HO1-axis such as STAT3 and p38
216 MAPK were found to be upregulated in a gene set enrichment analysis, **Figure 3f and g**. Another
217 immunosuppressive signaling marker closely related to the alternative activation of
218 macrophages/microglia is the release of TGF beta[21], which was also found to be up-regulated in highly
219 connected cells, **Figure 3g**.
220
221 **T cell Activation and Exhaustion Reveals Spatial Heterogeneity and Association with**
222 **Glioblastoma Subtype**
223 For glioblastoma, a tumor with a high degree of heterogeneity due to regional metabolic differences and
224 varying composition of the tumor microenvironment, the prediction of connected cells needs to be
225 confirmed by looking at the spatial overlapping of interacting cells. Mapping of spatial gene expression
226 is a novel technique used to overcome the limitation of scRNA-seq, which lacks spatial information,
227 **Figure 4a**. We performed spatial transcriptomic RNA sequencing (stRNA-seq) of 3 confirmed
228 glioblastomas of the IDH1/2 wild-type, containing a total number of 2,352 spots correctly aligned to the

H&E image, **Figure 4a**. We observed a median of 8 cells per spot (range: 4 to 22 cells per spot), which allows the spatial mapping of gene expression, but not at single cell resolution. However, when we compared our dataset to the recent classification of glioblastoma[22], consistent results were obtained in accordance to the diversity of subtype expression, **Figure 4b**. We used loess-fitted surface plots to map the gene set enrichment of either T cell activation (cluster 2) or T cell exhaustion (clusters 3 and 4), **Figure 4c-d**, which were highly heterogeneously distributed across patients. Whereas the first patient predominantly revealed areas with T cell exhaustion, **Figure 4d upper panel**, the others appeared more balanced, although the percentage of exhausted spots still dominated. Further, we showed the spatial overlap of the exhaustion marker genes (cluster 3) and IL10 response, **Figure 4e**. The spatial distribution was found to be consistent when using a published set of genes, which characterized the exhausted state of T cells. In a next step, we validated which expression subtype was spatially correlated with T cell exhaustion according to the novel molecular classification[22]. By overlaying the gene set expression and GBM subtype maps, we observed that "exhausted" regions were mainly occupied by mesenchymal regions, **Figure 4f**. We aligned all spots (sample 1-3) along a trajectory reflecting the enrichment of T cell exhaustion (using enrichment scores, detailed description in the methods), and mapped the signature genes of each molecular subtype for the same spot, **Figure 4g**. Thereby, we confirmed that in highly exhausted regions, signature genes of the mesenchymal subtype are also highly expressed.

Spatial Correlation of HMOX1$^+$-Myeloid Cells and T cell Exhaustion Signatures

With our NFCN-algorithm we screened for spots containing IL10 release and response and used both outputs to find overlapping regions within the spatial dataset, **Figure 5a**. The identified regions of high-IL10 signaling overlap with signatures reflecting T cell exhaustion (marker gene cluster 3) and marker genes of the connected cells identified above (*CD163*, *IL10*, *CD68*, *HMOX1*), **Figure 5b-c**. Furthermore, using the non-connected signatures (*IL1B*, *IL6*, *CD68*), we verify distinct localizations of myeloid states, **Figure 5c**. We observed a strong overlap between the connected cells and the expression of exhaustion markers, suggesting that our data confirm the interaction between HMOX1$^+$ myeloid cells and exhausted T cells.

Loss of Myeloid Cells Increases Antitumor Immunity

To further provide evidence for our findings from computational approach, we made use of recently described human neocortical slice model in which the cellular architecture of the CNS is well preserved [19,23]. We cultured non-infiltrated cortical slices (defined in a recent report[19,23]) with and without myeloid cell depletion, as recently described to understand the communication between myeloid cells in the tumor microenvironment along with lymphoid cells. Three days post depletion of myeloid cells using 11mM clodronate we injected a primary cell line (BTSC#233, GFP-tagged) characterized by RNA-seq profiling as mesenchymal[24]. Post tumor growth, we injected peripheral T cells (same donors), tagged by CellTrace™ Far Red (CTFR) and incubated the slices for another 24h, **Figure 6a**. By immunostaining we showed that myeloid cell depletion reduces the number of IBA1$^+$ cells along with most of HMOX1$^+$ cells, **Figure 6b**. Using enzyme-linked immunosorbent assay (ELISA) we found a significant reduction in IL10 when myeloid cells are depleted, regardless of the presence of tumor cells, **Figure 6c**. The strongest difference in IL10 release was observed between myeloid depleted slices in the presence of tumor cells, **Figure 6c**. Furthermore, we stained for Granzyme B (GZMB$^+$) T cells and quantified IL2 release to examine the amount of effector T cells in depleted or non-depleted slices. We found an increased number of GZMB$^+$ T cells in myeloid depleted slices, **Figure 6d**, along with significant increase of IL2 release, **Figure 6e.** Differences in IFN gamma release were not observed, **Figure 6f.** We also stained for the exhaustion marker TIM3 (Gen: *HAVCR2*), which was found to be enriched in exhausted T cells, and observed a loss of expression in the myeloid depleted slices, **Figure 6g**, suggesting that myeloid derived IL10 release (by HMOX1$^+$ cells) leads to T cell exhaustion, which is in line with the computational model.

Discussion:

Although single-cell RNA-sequencing accurately maps the cellular architecture and reflects the diversity of cellular states[17,22,25,26], spatial information is lacking. Here we combine single cell RNA sequencing of the immune compartment with spatial transcriptomic RNA-sequencing (stRNA-seq) to gain better insights into the complex crosstalk, cellular states and cellular plasticity leading to the immunosuppressive environment found in glioblastoma (GBM).

Recent studies have reported different subtypes of microglia and macrophages occupying glial tumors[1,4,22,25,26] although detailed information about the lymphoid infiltration cells is lacking. There is intense interest in T cells and their varied states due to their importance to the development of targeted therapies and understanding the immunosuppressive environment of glioblastoma. Currently available data characterizing T cell infiltration at the molecular level in glioblastoma (GBM) is limited. T cell states, particularly in disease, are somehow difficult to accurately classify, leading to numerous definitions and markers in recent years[2,7,27–29]. While some authors use the terms "dysfunctional" and "exhausted" synonymously[30], others differentiate between the dysfunctional and the exhausted states of T cells[27,29]. In this study we use the definition of cellular states released by Singer et al., 2016[8]. On the basis of these gene sets our data showed that only cells which remained activated along the pseudotime-trajectory were able to enter the state of dysfunction, and later exhaustion. The dysfunction appears to be a transitional state, associated with increased proliferation, despite immunosuppressive stimulation from the tumor environment. This imbalance between pro- and anti-inflammatory signaling, dominated by IL10 secretion, leads to final exhaustion of the T cells, which is in agreement with the current literature[2,31]. In order to find a consensus with regard to marker genes we further validated our findings on a set of exhausted marker genes recently published in an overview study[32]. We and others have shown that the environment of GBM aid the evolution of immune suppression. In this process, astrocytes and myeloid cells, both driven by STAT-3 signaling, orchestrate the immunosuppressive environment[4,19,33,34]. Based on the knowledge that IL10 interaction plays a crucial role in the shift from activated to exhausted T cells, we build an in-silico model that identified potential connected cells that drive the T cell exhaustion. By use of this model, we identified a subset of myeloid cells marked by high expression of *HMOX1*, a gene which is induced by oxidative stress and metabolic imbalance[35,36]. *HMOX1* is linked to the STAT-3 pathway and induces IL-10 production via MAPK activation and in agreement with the literature all of these markers were also found to be upregulated in our connected cells. Furthermore, we used the stRNA-seq to confirm the spatial overlap of cells which were identified

as highly connected. We showed that the *HMOX1*-myeloid cells were spatially correlated with exhaustion and the mesenchymal state of glioblastoma. These findings are accord with published reports, revealing that the mesenchymal cells are the component of GBM responsible for the immune crosstalk[22]. HMOX1 expression in GBM and IDH-WT astrocytoma was found to be increased in recurrent GBM and negatively associated with overall survival, **Supplementary Figure 5**. In addition, we made use of a human neocortical slice model with and without depletion of myeloid cells. By injecting tumor cells into the slices as well as T cells from the same donors, we simulated the function of the myeloid cells with regard to IL10 release and T cell stimulation. Fitting with our computational model, we confirmed that $HMOX1^{+}$ myeloid cells cause a reduction of effector T cells with a respective reduction in IL2 release and increased expression of our identified exhaustion marker TIM3.

The approach demonstrated here to integrate scRNA-seq and stRNA-seq using a variety of computational approaches does have some major limitations. First, the spatial transcriptomic array is only about 6 × 6.5 mm2 in size; therefore, the array can only show a limited portion of the actual tumor, and not every spot achieves single cell resolution. In this study we used first-generation spatial transcriptomic technology, meaning the number of spots, barcoding sensitivity and diffusion of transcripts across the spots is not fully optimized and needs more investigation for future datasets. Brain tissue, and GBM specimens respectively, are a challenge due to varying levels of tissue quality and problems with rapid RNA degradation. Despite the fact that we initially used 5 patients on the array with numerous validation and quality control experiments, the quality of the RNA and the library did not achieve our criteria for two of the patients. To date, brain tumor tissue has remained a challenge with this technique. Although we have performed numerous tissue optimization experiments to reduce transcript diffusion, the diffusion of transcripts through the spots during sample preparation cannot be totally avoided.

335 **Methods:**

336 **Ethical Approval**

337 The local ethics committee of the University of Freiburg approved the data evaluation, imaging
338 procedures and experimental design (protocol 100020/09 and 472/15_160880). The methods were
339 carried out in accordance with the approved guidelines, with written informed consent obtained from all
340 subjects. The studies were approved by an institutional review board. Further information and requests
341 for resources, raw data and reagents should be directed and will be fulfilled by the Contact: D. H.
342 Heiland, dieter.henrik.heiland@uniklinik-freiburg.de. A complete table of all materials used is given in
343 the supplementary information.

344

345 **T cell isolation and stimulation**

346 Blood was drawn from a healthy human individual into an EDTA (ethylenediaminetetraacetic acid)
347 cannula. T cells were extracted in a negative selection manner using a MACSxpress® Whole Blood Pan
348 T Cell Isolation Kit (Miltenyi Biotech). T cells were then transferred in Advanced RPMI 1640 Medium
349 (ThermoFisher Scientific, Pinneberg, Germany) and split for cytokine treatment: Three technical
350 replicates were used for each T cell-treatment condition. Interleukin 2 (IL-2, Abcam, Cambridge, UK)
351 was used at a final concentration of 1 ng/ml, Interleukin 10 (IL-10, Abcam) at 5 ng/ml, Interferon gamma
352 (IFN-γ, Abcam) at 1 ng/ml and Osteopontin (SPP-1, Abcam) at 3 µg/ml. Cytokine treatment was
353 performed in Advanced RPMI 1640 Medium and T cells were incubated at 37°C and 5% CO2 for 24h.

354

355 **RNA sequencing of stimulated T Cells**

356 The purification of mRNA from total RNA samples was achieved using the Dynabeads mRNA
357 Purification Kit (Thermo Fisher Scientific, Carlsbad, USA). The subsequent reverse transcription
358 reaction was performed using SuperScript IV reverse transcriptase (Thermo Fisher Scientific, Carlsbad,
359 USA). For preparation of RNA sequencing, the Low Input by PCR Barcoding Kit and the cDNA-PCR
360 Sequencing Kit (Oxford Nanopore Technologies, Oxford, United Kingdom) were used as recommended
361 by the manufacturer. RNA sequencing was performed using the MinION Sequencing Device, the
362 SpotON Flow Cell and MinKNOW software (Oxford Nanopore Technologies, Oxford, United Kingdom)
363 according to the manufacturer's instructions. Samples were sequenced for 48h on two flow-cells.
364 Basecalling was performed by Albacore implemented in the nanopore software. Only D^2-Reads with a
365 quality Score above 8 were used for further alignment.

366

367 **Sequence trimming and Alignment**

368 In the framework of this study, we developed an automated pipeline for nanopore cDNA-seq data, which
369 is available at github (https://github.com/heilandd/NanoPoreSeq). First the pipeline set up a new class
370 termed “Poreseq” by a distinct sample description file. The analysis starts by rearranging the reads from
371 the *fastq* output from the nanopore sequencer containing all of the D^2-Reads. All *fastq* files need to be
372 combined into one file. Multiplexed samples were separated according to their barcode and trimmed by
373 Porechop (https://github.com/rrwick/Porechop). Alignment was performed with minimap2
374 (https://github.com/lh3-/minimap2) and processed with sam-tools.

375

376 **Posthoc Analysis of Bulk-RNA-seq**

377 A matrix of counted genes was further prepared by the RawToVis.R
378 (github.com/heilandd/VRSD_Lab_v1.5) script containing, normalization of Mapped reads by DESeq,
379 batch effect removal (ComBat package) and fitting for differential gene expression. Gene set enrichment
380 analysis was performed by transformation of the log2 foldchange of DE into a ranked z-scored matrix
381 which was used as the input. The expression matrix was analysed with AutoPipe
382 (https://github.com/heilandd/AutoPipe) by a supervised machine-learning algorithm and visualized with
383 a heatmap. Full analysis was visualized by the Visualization of RNA-Seq Data (VRSD_Lab software,
384 github.com/heilandd/VRSD_Lab_v1.5) as a dashboard app based on shiny R-software. We extracted
385 the 50 top up/down regulated genes respectively of each stimulation with respect to control condition to
386 construct a stimulation library.

387

388 **Single-Cell Suspension for scRNA-sequencing**

389 Tumor tissue was obtained from glioma surgery immediately after resection and was transported in
390 Phosphate-buffered saline (PBS) in approximately 5 minutes into our cell culture laboratory. Tumor
391 tissue was processed under a laminar flow cabinet. Tissue was reduced to small pieces using two
392 scalpels and the tissue was processed with the Neural Tissue Dissociation Kit (T) using C-Tubes
393 (Miltenyi Biotech, Bergisch-Gladbach, Germany) according to the manufacturer´s instructions. The
394 Debris Removal Kit from Miltenyi was used according to the manufacturer´s instructions to remove
395 remaining myelin and extracellular debris. In order to remove the remaining erythrocytes, we
396 resuspended the pellet in 3,5 ml ACK lysis buffer (ThermoFisher Scientific, Pinneberg, Germany) and

incubated the suspension for 5 minutes followed by a centrifugation step (350g, 10 min, RT). Cell quantification with a hematocytometer was performed after discarding the supernatant and resuspending the pellet in PBS. Cell suspensions were centrifuged again (350g, 10 min, RT) and resuspended in freezing medium containing 10% DMSO (Sigma-Aldrich, Schnelldorf, Germany) in FCS (PAN-Biotech, Aidenbach, Germany). Cell suspensions were immediately placed in a freezing box containing isopropanol and stored in a -80°C freezer for not more than 4 weeks.

Cell sorting by Magnetic Beads

Four frozen single-cell suspensions, originating from one patient with an IDH-mutated glioma and three patients with an IDH-wildtype glioblastoma (GBM), were thawed and the dead cells were magnetically labeled and eliminated using a Dead Cell Removal Kit (Miltenyi Biotech). The tumor immune environment in general and T cells in particular were positively selected by using CD3+-MACS (Miltenyi Biotech). Cells were stained with trypan blue, counted using a hematocytometer and prepared at a concentration of 700 cells/µL.

Droplet scRNA-sequencing

At least 16000 cells per sample were loaded on the Chromium Controller (10x Genomics, Pleasanton, CA, USA) for one reaction of the Chromium Next GEM Single Cell 3´v3.1 protocol (10x Genomics), based on a droplet scRNA-sequencing approach. Library construction and sample indexing was performed according to the manufacturer´s instructions. scRNA-libraries were sequenced on a NextSeq 500/550 High Output Flow Cell v2.5 (150 Cycles) on an Illumina NextSeq 550 (Illumina, San Diego, CA, USA). The bcl2fastq function and the cell ranger (v3.0) was used for quality control.

Postprocessing scRNA-sequencing

We used cell ranger to detect low-quality read pairs of single-cell RNA sequencing (scRNA-seq) data. We filtered out reads which did not reach the following criteria: (1) bases with quality < 10, (2) no homopolymers (3) 'N' bases accounting for ≥10% of the read length. Filtered reads were mapped by STAR aligner and the resulting filtered count matrix further processed by Seurat v3.0 (R-package). We normalized gene expression values by dividing each estimated cell by the total number of transcripts and multiplied by 10,000, followed by natural-log transformation. Next, we removed batch effects and scaled data by a regression model including sample batch and percentage of ribosomal and

mitochondrial gene expression. For further analysis we used the 2000 most variable expressed genes and decomposed eigenvalue frequencies of the first 100 principal components and determined the number of non-trivial components by comparison to randomized expression values. The obtained non-trivial components were used for SNN clustering followed by dimensional reduction using the UMAP algorithm. Differently expressed genes (DE) of each cluster were obtained using a hurdle model tailored to scRNA-seq data which is part of the MAST package. Cell types were identified by 3 different methods; Classical expression of signature markers of immune cells; By SingleR an automated annotation tool for single-cell RNA sequencing data obtaining signatures from the Human Primary Cell Atlas, By SCINA, a semi-supervised cell type identification tool using cell-type signatures as well as a Gene-Set Variation Analysis (GSVA). Results were combined and clusters were assigned to the cell type with the highest enrichment within all models. In order to individually analyze T cells, we used the assigned cluster and filter for the following criteria. For further analysis T cells were defined by: $CD3^{+}CD8^{+}$ / $CD4^{+}CD14^{-}LYZ^{-}$ $GFAP^{-}CD163^{-}IBA^{-}$.

Spatial Transcriptomics

The spatial transcriptomics experiments were done using the 10X Spatial transcriptomics kit (https://spatialtranscriptomics.com/). All the instructions for Tissue Optimization and Library preparation were followed according to manufacturer's protocol. Here, we briefly describe the methods followed using the library preparation protocol.

Tissue collection and RNA quality control:

Tissue samples from three patients, diagnosed with WHO IV glioblastoma multiforme (GBM), were included in this study. Fresh tissue collected immediately post resection was quickly embedded in optimal cutting temperature compound (OCT, Sakura) and snap frozen in liquid N_2. The embedded tissue was stored at -80°C until further processing. A total of 10 sections (10μm each) per sample were lysed using TriZOl (Invitrogen, 15596026) and used to determine RNA integrity. Total RNA was extracted using PicoPure RNA Isolation Kit (Thermo Fisher, KIT0204) according to the manufacturer's protocol. RIN values were determined using a 2100 Bioanalyzer (RNA 6000 Pico Kit, Agilent) according to the manufacturer's protocol. It is recommended to only use samples with an RNA integrity value >7.

Tissue staining and Imaging:

Sections were mounted onto spatially barcoded glass slides with poly-T reverse transcription primers, with one section per array. These slides can be stored at -80°C until use. The slides were then warmed to 37°C, after which the sections were fixed for 10 minutes using 4% para-formaldehyde solution (Carl Roth, P087.1), which was then washed off using PBS. The fixed sections were covered with propan-2-ol (VWR, 20842312). Following evaporation for 40 seconds, sections were incubated in Mayer's Hematoxylin (VWR, 1092490500) for 7 min, bluing buffer (Dako, CS70230-2) for 90 seconds and finally in Eosin Y (Sigma, E4382) for 1 min. The glass slides were then washed using RNase/DNase free water and incubated at 37°C for 5 min or until dry. Before imaging, the glass slides were mounted with 87% glycerol (AppliChem, A3739) and covered with coverslips (R. Langenbrinck, 01-2450/1). Brightfield imaging was performed at 10x magnification with a Zeiss Axio Imager 2 Microscope, and post-processing was performed using ImageJ software.

The cover slips and glycerol were removed by washing the glass slides in RNase/DNase free water until the cover slips came off, after which the slides were washed using 80% ethanol to remove any remaining glycerol.

Permeabilization, cDNA synthesis and tissue removal:

For each capture array, 70µL of pre-permeabilization buffer, containing 50U/µL Collagenase along with 0.1% Pepsin in HCl was added, followed by an incubation for 20 minutes at 37°C. Each array well was then carefully washed using 100µL 0.1x SSC buffer. 70µL of Pepsin was then added and incubated for 11 minutes at 37°C. Each well was washed as previously described and 75µL of cDNA synthesis master mix containing: 96µL of 5X First strand buffer, 24 µL 0.1M DTT, 255.2µL of DNase/RNase free water, 4.8µL Actinomycin, 4.5µL of 20mg/mL BSA, 24µL of 10mM dNTP, 48µL of Superscript® and 24µL of RNAseOUT™ was added to each well and incubated for 20 hours at 42°C without shaking. Cyanine 3-dCTP was used to aid in the determination of the footprint of the tissue section used.

Since glioblastoma tissue is a fatty tissue, degradation and tissue removal was carried out using Proteinase K treatment for which 420µL Proteinase K and PKD buffer (1:7), were added to each well and then incubated at 56°C for 1hr with intermittent agitation (15 seconds / 3 minutes). After incubation, the glass slides were washed three times with 100mL of 50°C SSC/SDS buffer with agitation for 10 minutes, 1 minute and finally for 1 minute at 300 rpm. The glass slides were then air-dried at room

temperature. Tissue cleavage was carried out by the addition of 70μL of cleavage buffer (320μL RNase/DNase free water, 104μL Second strand buffer, 4.2μL of 10mM dNTP , 4.8μL of 20 mg/mL BSA and 48μL of USER™ Enzyme) to each well and incubation at 37°C for 2 hours with intermittent agitation.

Spot Hybridization:

In order to determine the exact location and quality of each of the 1007 spots, fluorescent Cyanine-3 A is hybridized to the 5' ends of the surface probes. 75μL of the hybridization solution (20μL of 10μM Cynaine-3A probe and 20μL of 10μM Cyanine-3 Frame probe in 960μL of 1X PBS) was added to each well and incubated for 10min at room temperature. The slides were then washed three times with 100ml of SSC/SDS buffer preheated to 50°C for 10min, 1min and 1min at room temperature with agitation. The slides were then air-dried and imaged after applying Slowfade® Gold Antifade medium and a cover slip.

Library Preparation:

1. Second Strand Synthesis

5μL second strand synthesis mix containing 20μL of 5X First Strand Buffer, 14μL of DNA polymerase I (10U/μL) and 3.5μL Ribonuclease H (2U/μL) were added to the cleaved sample and incubated at 16°C for 2 hours. Eppendorf tubes were placed on ice and 5μL of T4 DNA polymerase (3U/μL) were added to each strand and incubated for 20 minutes at 16°C. 25μL of 80mM EDTA (mix 30μL of 500mM EDTA with 158μL DNase/RNase free water) was added to each sample and the samples were kept cool on ice.

2. cDNA purification

cDNA from the previous step was purified using Agencourt RNAclean XP beads and DynaMag™- 2 magnetic rack, incubated at room temperature for 5 min. Further cleansing was performed by the addition of 80% Ethanol to the sample tubes, while the samples were still placed in the magnetic rack. Sample elution was then carried out using 13μL of NTP/water mix.

3. In Vitro Transcription and Purification

cDNA transcription to aRNA was carried out by adding 4μL of reaction mix containing: 10x Reaction Buffer, T7 Enzyme mix and SUPERaseIn™ RNase Inhibitor (20 U/μL) to 12μL of the eluted cDNA sample and incubated at 37°C, for 14 hours. The samples were purified using RNA clean XP beads

519 according to the manufacturer's protocol and further eluted into 10μL DNase/RNase free water. The
520 amount and average fragment length of amplified RNA was determined using the RNA 6000 Pico Kit
521 (Agilent, 5067-1513) with a 2100 Bioanalyzer according to the manufacturer's protocol.

522 **4. Adapter Ligation**

523 Next, 2.5μL Ligation adapter (IDT) was added to the sample and was heated for 2 min at 70°C and then
524 placed on ice. A total of 4.5μL ligation mix containing 11.3μL of 10X T4 RNA Ligase, T4 RNA truncated
525 Ligase 2 and 11.3μL of murine RNase inhibitor was then added to the sample. Samples were then
526 incubated at 25°C for 1 hour. The samples were then purified using RNAClean XP beads according to
527 the manufacturer's protocol.

528 **5. Second cDNA synthesis**

529 Purified samples were mixed with 1μL cDNA primer (IDT), 1μL dNTP mix up to a total volume of 12μL
530 and incubated at 65°C for 5 min and then directly placed on ice. A 1.5ml Eppendorf tube 8μL of the
531 sample was mixed with 30μL of First Strand Buffer(5X),), 7.5μL of DTT(0.1M), 7.5μL of DNase/RNase
532 free water, 7.5μL of SuperScript® III Reverse transcriptase and 7.5μL of RNaseOUT™ Recombinant
533 ribonuclease Inhibitor and incubated at 50°C for 1 hour followed by cDNA purification using Agencourt
534 RNAClean XP beads according to the manufacturer's protocol. Samples were then stored at -20°C.

535 **6. PCR amplification**

536 Prior to PCR amplification, we determined that 20 cycles were required for appropriate amplification. A
537 total reaction volume of 25μL containing 2x KAPA mix, 0.04μM PCRInPE2 (IDT), 0.4μM PCR InPE1.0
538 (IDT), 0.5μM PCR Index (IDT) and 5μL of purified cDNA were amplified using the following protocol:
539 98°C for 3 min followed by 20 cycles at 98°C for 20 seconds, 60°C for 30 seconds , 72°C for 30 seconds
540 followed by 72°C for 5 minutes. The libraries were purified according to the manufacturer's protocol and
541 eluted in 20μL EB (elution buffer). The samples were then stored at -20°C until used.

542 **7. Quality control of Libraries**

543 The average length of the prepared libraries was quantified using a Agilent DNA 1000 high sensitivity
544 kit with a 2100 Bioanalyzer. The concentration of the libraries was determined using a Qubit dsDNA HS
545 kit. The libraries were diluted to 4nM, pooled and denatured before sequencing on the Illumina NextSeq
546 platform using paired end sequencing. We used 30 cycles for read 1 and 270 cycles for read 2 during
547 sequencing.

	Sequence
Ligation Adapter	/5rApp/AGATCGGAAGAGCACACGTCTGAACTCCAGTCAC/3d- dC/
cDNA primer	GTGACTGGAGTTCAGACGTGTGCTCTTCCGA
PCR primer INPE1	AATGATACGGCGACCACCGAGATCTACACTCTTTCCCTACACGACGCTCTT-CCGATCT
PCR primer INPE2	GTGACTGGAGTTCAGACGTGTGCTCTTCCGATCT
PCR index primer	CAAGCAGAAGACGGCATACGAGATCGTGATGTGACTGGAGTTC

Postprocessing Spatial Transcriptomics

First, we aligned the H&E staining by the use of the st-pipeline (github.com/SpatialTranscriptomics-Research/st_pipeline). The pipeline contains the following steps: Quality trimming and removing of low quality bases (bases with quality < 10), sanity check (reads same length, reads order, etc..), remove homopolymers, normalize for AT and GC content, mapping the read2 with STAR, demultiplexing based on read1, sort for reads (read1) with valid barcodes, annotate the reads with htseq-count, group annotated reads by barcode (spot position), gene and genomic location (with an offset) to get a read count (github.com/SpatialTranscriptomics-Research/st_pipeline). The pipeline resulted in a gene count matrix and a spatial information file containing the x and y position and the H&E image. We used the Seurat v3.0 package to normalize gene expression values by dividing each estimated cell by the total number of transcripts and multiplied by 10,000, followed by natural-log transformation. As described for sc-RNA sequencing, we removed batch effects and scaled data by a regression model including sample batch and percentage of ribosomal and mitochondrial gene expression. For further analysis we used the 2000 most variable expressed genes and decomposed eigenvalue frequencies of the first 100 principal components and determined the number of non-trivial components by comparison to randomized expression values. The obtained non-trivial components were used for SNN clustering followed by dimensional reduction using the UMAP algorithm. Differently expressed genes (DE) of each cluster were obtained using a hurdle model tailored to scRNA-seq data which is part of the MAST package. We further build a user-friendly viewer for spatial transcriptomic data (ST__Lab_v1.4), available at github (github.cm/heilandd/ST_Lab). The software tool contains various visualization options: Dimensional reduction given by the UMAP, spatial plots (spatial gene expression), state plots (scatter plots representative for subgroups reactive states of cells) and spatial correlation (further details given in the separate sections)

573

574

575 **Spatial gene expression**

576 For spatial expression plots, we used either normalized and scaled gene expression values (to plot
577 single genes) or scores of a set of genes, using the 0.5 quantile of a probability distribution fitting. The
578 x-axis and y-axis coordinates are given by the input file based on the localization at the H&E staining.
579 We computed a matrix based on the maximum and minimum extension of the spots used (32x33)
580 containing the gene expression or computed scores. Spots without tissue covering were set to zero.
581 Next, we transformed the matrix, using the squared distance between two points divided by a given
582 threshold, implemented in the fields package (R-software) and adapted the input values by increasing
583 the contrast between uncovered spots. The data are illustrated as surface plots (plotly package R-
584 software) or as images (graphics package R-software).

585

586 **Representation of Cellular States**

587 We aligned cells/spots to variable states regarding to gene sets (GS) that were selected $GS_{(1,2,..n)}$. First,
588 we separated cells into $GS_{(1+2)}$ versus $GS_{(2+4)}$, using the following equation:

589 $$A_1 = \| GS_{(1)}, GS_{(2)} \|_\infty - \| GS_{(3)}, GS_{(4)} \|_\infty$$

590 A1 defines the y-axis of the two-dimensional representation. In a nest step, we calculated the x-axis
591 separately for spots $A1<0$ and $A1>0$:

592 $$A1 > 0: A_2 = \log 2 \, (\overline{GS_{(1)}} - \lceil \overline{GS_{(2)}} + 1 \rceil)$$

593 $$A1 < 0: A_2 = \log 2 \, (\overline{GS_{(3)}} - \lceil \overline{GS_{(4)}} \rceil)$$

594 For further visualization of the enrichment of subsets of cells according to gene set enrichment across
595 the two-dimensional representation, using a probability distribution fitting we transformed the distribution
596 to representative colors. This representation is an adapted method published by Neftel and colleges
597 recently[22,26].

598

599 **Spatial correlation analysis**

600 In order to map spatial correlated gene expression or gene set enrichments we used z-scored ranked
601 normalized expression values. One gene expression vector or enrichment vector of a gene set is used
602 to order the spots along a spatial trajectory. We construct the trajectory of spots from lowest ranked to
603 highest ranked spot (based on z-scored input vectors). The genes of interest (which were correlated

with the spatial trajectory) are fitted by loess-fit from the stats-package (R-software) and aligned to the ranked spots and scaled. Correlation analysis was performed by Pearson's product moment correlation coefficient. For heatmap illustration the gene order was computed by ordering the maximal peak of the loess fitted expression along the predefined spatial trajectory.

Pseudotime trajectory analysis

We down-scaled all 5 clusters of T cells to a total number of 1,500 cells as input for Single-cell Trajectories Reconstruction, Exploration And Mapping (STREAM). Normalized counts were used as input. We performed 10 replications of randomized down-scaling and STREAM trajectory reconstruction. We used STREAM mapping to identify transition genes (genes with reasonable dynamic along the inferred pseudotime) as well as leaf genes (genes with significant enrichment in a single leaf), this is further used to reconstruct cell fate decisions along the inferred pseudotime. Pseudotime analysis were illustrated as stream plots or subway plots (from the STREAM pipeline) or as heatmaps. To build the heatmap, we aligned each cell along their inferred pseudotime position and fitted the normalized gene expression. Then we created z-scores for each gene and plot genes by pheatmap function (pheatmap package, R-software). Genes were ordered by a correlation trajectory of the maximum peak of the fitted expression and the inferred pseudotime.

Gene set enrichment analysis

Gene sets were obtained from the database MSigDB v7 and internally created gene sets are available at githunb.com/heilandd. For enrichment analysis of single clusters, the normalized and centered expression data were used and further transformed to z-scores ranging from 1 to 0. Genes were ranked in accordance to the obtained differential expression values and used as the input for GSEA.

Identification of cycling cells

We used the set of genes published by Neftel and colleagues to calculate proliferation scores based on the GSVA package implemented in R-software. The analysis based on a non-parametric unsupervised approach, which transformed a classic gene matrix (gene-by-sample) into a gene set by sample matrix resulted in an enrichment score for each sample and pathway. From the output enrichment scores we set a threshold based on distribution fitting to define cycling cells.

635

636

637 **Nearest Functionally Connected Neighbor (NFCN)**

638 To identify connected cells that interact by defined activation or inhibition of down-stream signals in the
639 responder cell, we created a novel model. Therefore, we assumed that a cell-cell interaction is given
640 only if a receptor/ligand pair induce correspondent down-stream signaling within the responder cell (cell
641 with expressed receptor). Furthermore, we take into account that the importance of an activator cell (cell
642 with expressed ligand) can be ranked according to their enriched signaling, which is responsible for
643 inducing ligand expression. Based on these assumptions we defined an algorithm to map cells along an
644 interaction-trajectory. The algorithm was designed to identify potential activators from a defined subset
645 of cells.
646 As input for the analysis we used a normalized and scaled gene expression matrix, a string containing
647 the subset of target cells, a list of genes defining ligand induction on the one side and receptor signaling
648 on the other side. These genes were chosen either by the MSigDB v7 database or our stimulation library
649 explained above. Then, we down-scaled the data to 3000 representative cells including all myeloid cell
650 types and calculate the enrichment of induction and activation of the receptor/ligand pair. Enrichment
651 scores were calculated by singular value decomposition (SVD) over the genes in the gene set and the
652 coefficients of the first right-singular vector defined the enrichment of induction/activation profile. Both
653 expression values and enrichment scores were fitted by a probability distribution model and cells outside
654 the 95% quantile were removed. Next, we fitted a model using a non-parametric kernel estimation
655 (Gaussian or Cauchy-Kernel), on the basis of receptor/ligand expression (A_{exp}) and up/downstream
656 signaling (A_{eff}) of each cell ($i=\{1,..n\}$). Both input vectors were normalized and z-scored:

657

658 $$(1)\ n_{\exp i} = \frac{A_{\exp i} - min(A_{exp})}{max(A_{exp}) - min(A_{exp})} \qquad (2)\ \hat{f}_h(n_{\exp i}) = \frac{1}{n}\sum_{i=1}^{n} K_h(n_{exp} - n_{\exp i})$$

659

660 K is the kernel and 0.7 > h > 0.3 is used to adjust the estimator. The model result in a trajectory which
661 were defined as $\mathrm{Ligand}^{(\cdot)}$-$\mathrm{Induction}^{(\cdot)}$ to cells of the target subset with $\mathrm{Receptor}^{(\cdot)}$-$\mathrm{Activation}^{(\cdot)}$.Further
662 cells were aligned along the “interaction-trajectory”. We defined connected cells by reaching the upper
663 70% CI in receptor/ligand expression as well as sores of induction/activation. The way of representation
664 is illustrated schematically in **Figure 3a**.

665

CNV estimation:

Copy-number Variations (CNVs) were estimated by aligning genes to their chromosomal location and applying a moving average to the relative expression values, with a sliding window of 100 genes within each chromosome, as described recently[17]. First, we arranged genes in accordance to their respective genomic localization using the CONICSmat package (R-software). As a reference set of non-malignant cells, we in-silico extracted 400 CD8 positive cells (unlikely to be expressed on tumor cells). To avoid the considerable impact of any particular gene on the moving average we limited the relative expression values [-2.6,2.6] by replacing all values above/below $exp_{(i)}$=|2.6|, by using the infercnv package (R-software). This was performed only in the context of CNV estimation as previous reported[11].

Flow cytometry:

Single-Cell suspensions were obtained after Dead-Cell Removal and CD3 MACS-enrichment. Cells were incubated with VivaFix™ 398/550 (BioRad Laboratories, CA, USA) according to the manufacturer´s instructions. Cells were fixed in 4% paraformaldehyde (PFA) for 10 minutes. After centrifugation (350 g; 4°C; 5 min) and removal of the supernatant, the cell pellet was suspended in 0.5 ml 4°C cold FACS buffer. Cell suspension were washed and centrifuged at 350xg for 5 mins, followed by resuspension in FACS buffer. The washing step was repeated twice. Finally, cells were resuspended in at least 0.5 to 1 mL of FACS buffer depending on the number of cells. We used a Sony SP6800 spectral analyzer in standardization mode with PMT voltage set to maximum to reach a saturation rate below 0.1 %. Gating was performed by FCS Express 7 plus at the core facility, University of Freiburg.

Immunofluorescence

The same protocol was followed for human neocortical slices with or without microglia and tumor cell injection. The media was removed and exchanged for 1 mL of 4% paraformaldehyde (PFA) for 1 h and further incubated in 20% methanol in PBS for 5 minutes. Slices were then permeabilized by incubating in PBS supplemented with 1 % Triton (TX-100) overnight at 4°C and further blocked using 20% BSA for 4 hours. The permeabilized and blocked slices were then incubated by primary antibodies in 5% BSA-PBS incubated overnight at 4°C. After washing in PBS, slices were labelled with secondary antibodies conjugated with Alexa 405, 488, 555, or 568 for 3 hours at room temperature. Finally, slices were

mounted on glass slides using DAPI fluoromount (Southern Biotech, Cat. No. 0100-20), as recently described[19].

Human Organotypic Slice Culture

Human neocortical slices were prepared as recently described[19,23]. Capillaries and damaged tissue were dissected away from the tissue block in the preparation medium containing: Hibernate medium supplemented with 13 mM D+ Glucose, 30 mM NMDG and 1 mM Glutamax. Coronal slices of 300 μm thickness were sectioned using a vibratome (VT1200, Leica Germany) and incubated in preparation medium for 10 minutes before plating to avoid any variability due to tissue trauma. Three to four slices were gathered per insert. The transfer of the slices was facilitated by a polished wide mouth glass pipette. Slice were maintained in growth medium containing Neurobasal (L- Glutamine) supplemented with 2% serum free B-27, 2% Anti- Anti, 13 mM D+ Glucose, 1 mM MgSO4, 15 mM HEPES (Sigma, H0887) and 2 mM Glutamax at 5% CO_2 and 37 °C. The entire medium was replaced with fresh culture medium 24 hours post plating and every 48 hours thereafter.

Chemical depletion of Microglia from slice cultures

Selective depletion of myeloid cell compartment in human neocortical slices was performed by supplementing the growth medium with 11 µmol of Clodronate (Sigma, D4434) for 72h at 37ºC. Subsequently, the slices were carefully rinsed with growth medium to wash away any debris.

Tumor/T cell injection onto tissue cultures

ZsGreen tagged BTSC#233 cell lines cultured and prepared as described in the cell culture section. Post trypsinization, a centrifugation step was performed, following which the cells were harvested and suspended in MEM media at 20,000 cells/µl. Cells were used immediately for injection onto tissue slices. A 10 µL Hamilton syringe was used to manually inject 1 µL into the white matter portion of the slice culture. Slices with injected cells were incubated at 37°C, 5% CO2 for 7 days and fresh culture medium was added every 2 days. Blood samples from the same donors from whom we obtained the healthy cortex for our organotypic slice cultures was drawn into an EDTA-cannula. Peripheral T cells were isolated using the same MACSxpress® Whole Blood Pan T Cell Isolation Kit (Miltenyi Biotech). T cells were tagged using the Cell Trace Far Red dye (ThermoFisher Scientific) prior to injection into the slices. Erythrocytes were eliminated from the suspension using ACK-lysis buffer (Thermo Fisher Scientific).

728

729 **Enzyme linked Immunosorbent Assay**

730 An enzyme linked immunosorbent assay (ELISA) was performed in order to measure cytokine
731 concentrations of IL-2, IL-10, IL-13 and IFN-gamma in the cell culture medium 24h after T cell injection.
732 The Multi-Analyte ELISArray Kit (Qiagen, Venlo, Netherlands; MEH-003A) was used according to the
733 manufacturer´s instructions. Absorbances were measured using the Tecan Infinite® 200 (Tecan,
734 Männedorf, Switzerland).

735

736 **Acknowledgement**

737 DHH is funded by the German Cancer Society (Seeding Grand TII), Müller-Fahnenberg Stiftung and
738 Familie Mehdorn Stiftung. We thank Manching Ku and Dietmar Pfeifer for here helpful advices.

739

740 **Conflict of interests**

741 No potential conflicts of interest were disclosed by the authors.

742

743 **Data availability**

744 scRNA-Sequencing Data available: (in preparation), Accession codes: www.github.com/heilandd/.
745 VisLabv1.5 https://github.com/heilandd/Vis_Lab1.5, NFCN Algorithm www.github.com/heilandd/NFCN,
746 SPATA-Lab: www.github.com/heilandd/-SPATA-Lab. Further information and requests for resources,
747 raw data and reagents should be directed and will be fulfilled by the Contact: D. H. Heiland,
748 dieter.henrik.heiland@uniklinik-freiburg.de.

749

750

Bibliography

1. Darmanis, S. *et al.* Single-Cell RNA-Seq Analysis of Infiltrating Neoplastic Cells at the Migrating Front of Human Glioblastoma. *Cell Rep.* **21,** 1399–1410 (2017).
2. Woroniecka, K. *et al.* T-Cell Exhaustion Signatures Vary with Tumor Type and Are Severe in Glioblastoma. *Clin. Cancer Res.* **24,** 4175–4186 (2018).
3. Chen, Z. & Hambardzumyan, D. Immune microenvironment in glioblastoma subtypes. *Front. Immunol.* **9,** 1004 (2018).
4. Sankowski, R. *et al.* Mapping microglia states in the human brain through the integration of high-dimensional techniques. *Nat. Neurosci.* **22,** 2098–2110 (2019).
5. Zhang, L. *et al.* Lineage tracking reveals dynamic relationships of T cells in colorectal cancer. *Nature* **564,** 268–272 (2018).
6. Zheng, C. *et al.* Landscape of Infiltrating T Cells in Liver Cancer Revealed by Single-Cell Sequencing. *Cell* **169,** 1342–1356.e16 (2017).
7. Baitsch, L. *et al.* Exhaustion of tumor-specific $CD8^+$ T cells in metastases from melanoma patients. *J. Clin. Invest.* **121,** 2350–2360 (2011).
8. Singer, M. *et al.* A Distinct Gene Module for Dysfunction Uncoupled from Activation in Tumor-Infiltrating T Cells. *Cell* **166,** 1500–1511.e9 (2016).
9. Anderson, A. C., Joller, N. & Kuchroo, V. K. Lag-3, Tim-3, and TIGIT: Co-inhibitory Receptors with Specialized Functions in Immune Regulation. *Immunity* **44,** 989–1004 (2016).
10. Im, S. J. *et al.* Defining CD8+ T cells that provide the proliferative burst after PD-1 therapy. *Nature* **537,** 417–421 (2016).
11. Tirosh, I. *et al.* Dissecting the multicellular ecosystem of metastatic melanoma by single-cell RNA-seq. *Science* **352,** 189–196 (2016).
12. Platten, M., Ochs, K., Lemke, D., Opitz, C. & Wick, W. Microenvironmental clues for glioma immunotherapy. *Curr Neurol Neurosci Rep* **14,** 440 (2014).
13. Filley, A. C., Henriquez, M. & Dey, M. Recurrent glioma clinical trial, CheckMate-143: the game is not over yet. *Oncotarget* **8,** 91779–91794 (2017).
14. Weller, M. *et al.* Rindopepimut with temozolomide for patients with newly diagnosed, EGFRvIII-expressing glioblastoma (ACT IV): a randomised, double-blind, international phase 3 trial. *Lancet Oncol.* **18,** 1373–1385 (2017).
15. Zhang, Z. *et al.* SCINA: A Semi-Supervised Subtyping Algorithm of Single Cells and Bulk Samples. *Genes (Basel)* **10,** (2019).
16. Aran, D. *et al.* Reference-based analysis of lung single-cell sequencing reveals a transitional profibrotic macrophage. *Nat. Immunol.* **20,** 163–172 (2019).
17. Patel, A. P. *et al.* Single-cell RNA-seq highlights intratumoral heterogeneity in primary glioblastoma. *Science* **344,** 1396–1401 (2014).
18. Chen, H. *et al.* Single-cell trajectories reconstruction, exploration and mapping of omics data with STREAM. *Nat. Commun.* **10,** 1903 (2019).
19. Henrik Heiland, D. *et al.* Tumor-associated reactive astrocytes aid the evolution of immunosuppressive environment in glioblastoma. *Nat. Commun.* **10,** 2541 (2019).

20. Naito, Y., Takagi, T. & Higashimura, Y. Heme oxygenase-1 and anti-inflammatory M2 macrophages. *Arch. Biochem. Biophys.* **564,** 83–88 (2014).
21. Qin, Y. *et al.* A Milieu Molecule for TGF-β Required for Microglia Function in the Nervous System. *Cell* **174,** 156–171.e16 (2018).
22. Neftel, C. *et al.* An integrative model of cellular states, plasticity, and genetics for glioblastoma. *Cell* **178,** 835–849.e21 (2019).
23. Ravi, V. M. *et al.* Human organotypic brain slice culture: a novel framework for environmental research in neuro-oncology. *Life Sci. Alliance* **2,** (2019).
24. Kling, T. *et al.* Integrative Modeling Reveals Annexin A2-mediated Epigenetic Control of Mesenchymal Glioblastoma. *EBioMedicine* **12,** 72–85 (2016).
25. Venteicher, A. S. *et al.* Decoupling genetics, lineages, and microenvironment in IDH-mutant gliomas by single-cell RNA-seq. *Science* **355,** (2017).
26. Tirosh, I. *et al.* Single-cell RNA-seq supports a developmental hierarchy in human oligodendroglioma. *Nature* **539,** 309–313 (2016).
27. Blank, C. U. *et al.* Defining “T cell exhaustion”. *Nat. Rev. Immunol.* **19,** 665–674 (2019).
28. Jiang, Y., Li, Y. & Zhu, B. T-cell exhaustion in the tumor microenvironment. *Cell Death Dis.* **6,** e1792 (2015).
29. Wherry, E. J. T cell exhaustion. *Nat. Immunol.* **12,** 492–499 (2011).
30. Li, H. *et al.* Dysfunctional CD8 T Cells Form a Proliferative, Dynamically Regulated Compartment within Human Melanoma. *Cell* **176,** 775–789.e18 (2019).
31. Woroniecka, K. I., Rhodin, K. E., Chongsathidkiet, P., Keith, K. A. & Fecci, P. E. T-cell Dysfunction in Glioblastoma: Applying a New Framework. *Clin. Cancer Res.* **24,** 3792–3802 (2018).
32. Winkler, F. & Bengsch, B. Use of mass cytometry to profile human T cell exhaustion. *Front. Immunol.* **10,** 3039 (2019).
33. Wurm, J. *et al.* Astrogliosis Releases Pro-Oncogenic Chitinase 3-Like 1 Causing MAPK Signaling in Glioblastoma. *Cancers (Basel)* (2019).
34. Priego, N. *et al.* STAT3 labels a subpopulation of reactive astrocytes required for brain metastasis. *Nat. Med.* **24,** 1024–1035 (2018).
35. Kaiser, S. *et al.* Neuroprotection after Hemorrhagic Stroke Depends on Cerebral Heme Oxygenase-1. *Antioxidants (Basel)* **8,** (2019).
36. Sebastián, V. P. *et al.* Heme Oxygenase-1 as a Modulator of Intestinal Inflammation Development and Progression. *Front. Immunol.* **9,** 1956 (2018).

Figure Description:

Figure 1: a) Illustration of the workflow, tissue specimens are obtained from 7 glioblastoma patients while 4 patients were used for scRNA-seq and 3 patients for spatial transcriptomics. **b)** Dimensional reduction using UMAP, cell type was determined by SingleR (github.com/dviraran/SingleR) and SCINA[15]. **c)** Dimensional reduction (UMAP) of $CD3^{+}/CD8^{+}$ cells. SNN-clustering reveal 5 different cluster (upper panel). Pseudotime analysis by single-cell trajectory reconstruction exploration and mapping (STREAM) revealed 3 branches (bottom panel). **d)** Heatmap of mean single sample GSEA computed by gene set variation analysis using the C2/C5 /hallmark and C7 gene sets from the MSigDB and ImmuneSigDB. Differential activation was illustrated by common markers of naive, effector or exhausted T cells (Dimensional reduction (UMAP) of gene expression, right side). **e)** Dimensional reduction (UMAP) of gene expression of proliferation marker *MKI67* and *TOP2A* and GSEA plots illustrate the proliferative capacity of different clusters. **f)** Arrangement of clusters along the pseudotime illustrated in a subway-plot (STREAM). **g)** Subway plot from the STREAM analysis illustrate the expression of *TOP2A* as marker for proliferation **h)** GSEA plots indicating IL10 and IFNG response in C1-4. **i)** Pseudotime enrichment of signature genes of exhaustion or T cell activation[8], in the upper panel, scGSEA of the IFNG and IL10 response is shown. At bottom, an illustration of the pseudotime arrangement indicates the organization of cells in the heatmap.

Figure 2: a) Workflow to build a library of stimulated T-cells b) T cell stimulation in order to build a library for cytokine effects, illustrated is a heatmap of the 10 most significant marker genes of each stimulation state, based on PAMR algorithm implemented in the AutoPipe. c) Gene Set Enrichment curves of top 50 up-regulated genes of the IL-10 and IL-2 stimulation. Enrichment was validated in the different cluster from our scRNA-seq. d) Heatmap of different stimulation states, mapped are genes of the four clusters.

Figure 3: **a)** Workflow to explore cell-cell interactions **b)** Cell-cell interaction plot as explained in a). Cells with an interaction-score above 0.8 are mapped to the UMAP. **c)** A UMAP illustration with representative connected cells, in the upper panels only the strongest connected cells (quantile over 90%) at the bottom panels, the UMAP presentation with connection above the 80% and 70% quantile. **d)** Circular plot indicates the different T cell cluster (right side) and myeloid cluster (left side). Bar charts indicate the percentage of cells in their respective clusters, for IL10-Receptor cells (right) and IL-10 Ligand cells

(left), Fisher's exact test was used for statistical testing. **e)** Volcano plot of differential gene expression between highly connected cells (CI>97.5%, left side) vs non-connected cells (CI<2.5%, right side), adjusted -log(p-vale) (FDR) was used at the y-axis. Red cells are defined by fold-change above 2 and FDR < 0.05. **f)** Violin plots of gene expression between connected cells (CI>97.5%, left side) vs non-connected cells (CI<2.5%, right side). Wilcoxon Rank Sum test and FDR adjustment was used for statistical testing. **g)** Gene Set enrichment analysis of four different gene sets.

Figure 4: **a)** Workflow of spatial transcriptomics **b)** 2D representation of heterogeneity states of glioblastoma by Neftel, colors indicate the expression of cycling cells (quantile). **c)** H&E stainings and correspondent gene expression profiles **(d)** with spatial distribution of T cell exhaustion (signature cluster 3-4, in red) and T cell activation (cluster 2, green). **e-f)** Spatial gene expression map of signature genes of cluster 3 (left top) or IL-10 stimulation (right top), map of tumor heterogeneity in accordance to the signature of Neftel et al., 2019. **g)** Heatmap of spots mapped along a trajectory that represents T cell exhaustion, the heatmap shows the gene expression of subtype signature genes (indicated at the left side).

Figure 5: **a-b)** Cell-cell interaction plot as explained in Figure 4a). Cells with an interaction-score above 0.8 are mapped to the spatial position and the density of connectivity is given in b) as a heatmap. c)Spatial gene expression maps of all patients with enrichment of exhaustion (Cluster3) in the upper panel and inflammatory-alternative activated phenotype of myeloid cells in the bottom part.

Figure 6: a) Experimental workflow of the neocortical slice model with and without myeloid cell depletion. b) Immunostainings of IBA1 (Macrophages and Microglia) in magenta and HMOX1 in cyan, tumor cells are illustrated by grey. In the upper panel, the control set with maintained myeloid cells (M^+) is shown, the bottom panel contains the myeloid cell depleted slices. c) Cytokine level of IL10 measured by ELISA from the medium. d) Immunostainings of T cells (CSFE-Tagged, in red) and GZMB a marker of T cell activation (green). e-f) ELISA measurements of IL2 and IFNg. g) Immunostainings of TIM3 (gene: *HAVCR2*) in yellow, which was identified in the scRNA-seq, and T cell in red. P-values are determined by one-way ANOVA (c,e,f) adjusted by Benjamini-Hochberger (c,e,f) for multiple testing. Data is given as mean ± standard deviation.

Supplementary Figures:

Supplementary Figure1: a) UMAP representation of all cluster. b) Correlation matrix of all clusters c-d) Distribution of cell types and patients across all clusters. e) Signature genes of each cluster f) UMAP representation of signature cell type markers.

Supplementary Figure2: a) Copy-number alterations based on single cell data. Only a small subset of tumor cells was found in the OPC cluster.

Supplementary Figure3: a) Heatmap indicates marker genes of different T cell states. b) UMAP presentation of T cell clusters with color-coded expression of the Singer signatures of T cell states. c) Dimensional reduction (UMAP) of gene expression of CTLA4 and PDCD1 as well IFNG and GZMB (d).

Supplementary Figure4: a) Dimensional reduction (UMAP) of gene expression in the full sc-dataset. Colors indicate gene expression across all clusters.

Supplementary Figure5: a) Kaplan-Meier survival estimation of HMOX1 high/low expression GBM. b-c) Expression of HMOX1 in different regions of the tumor (b) and in de-novo and recurrent stage (c).

Figure 1

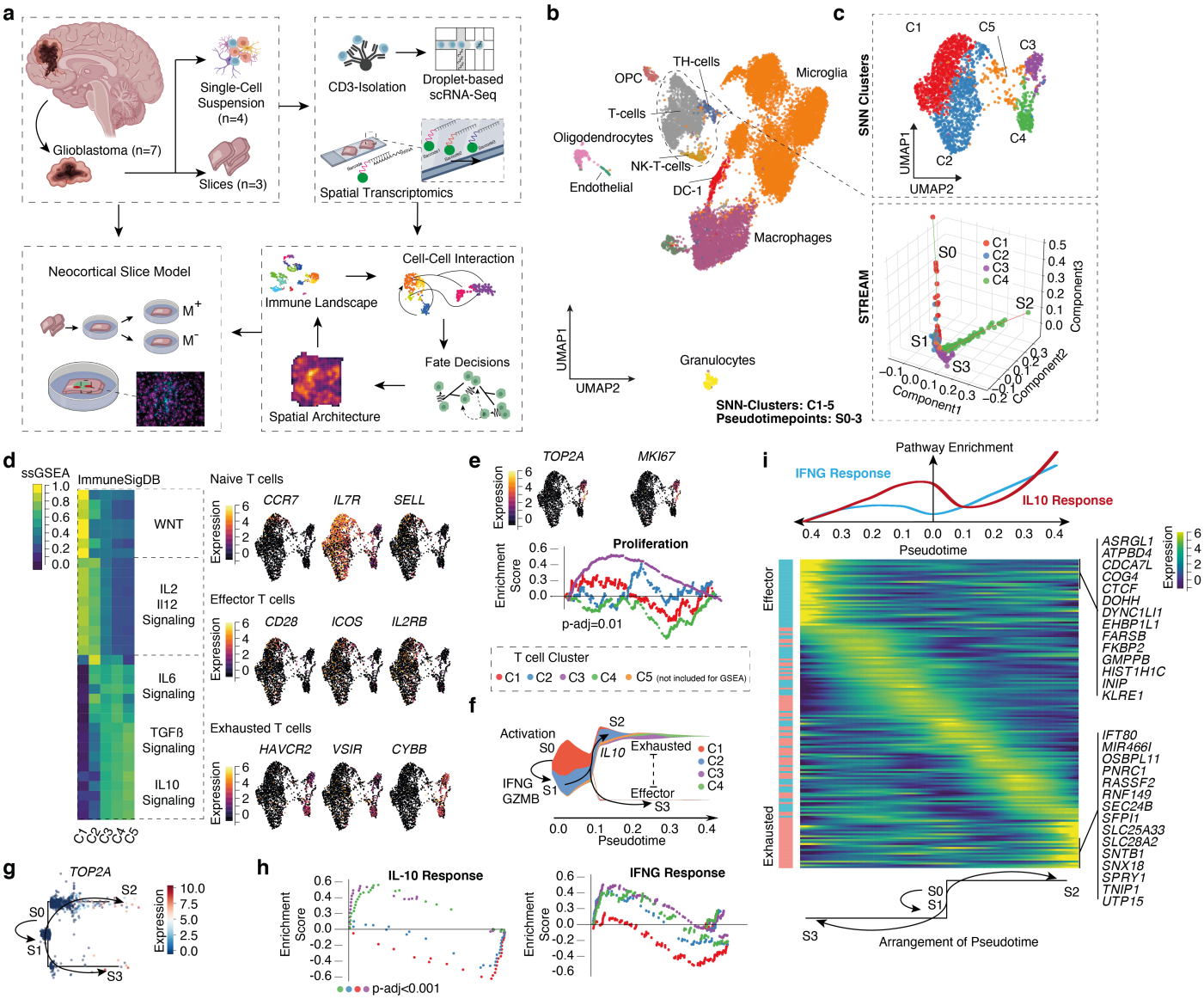

Figure 2

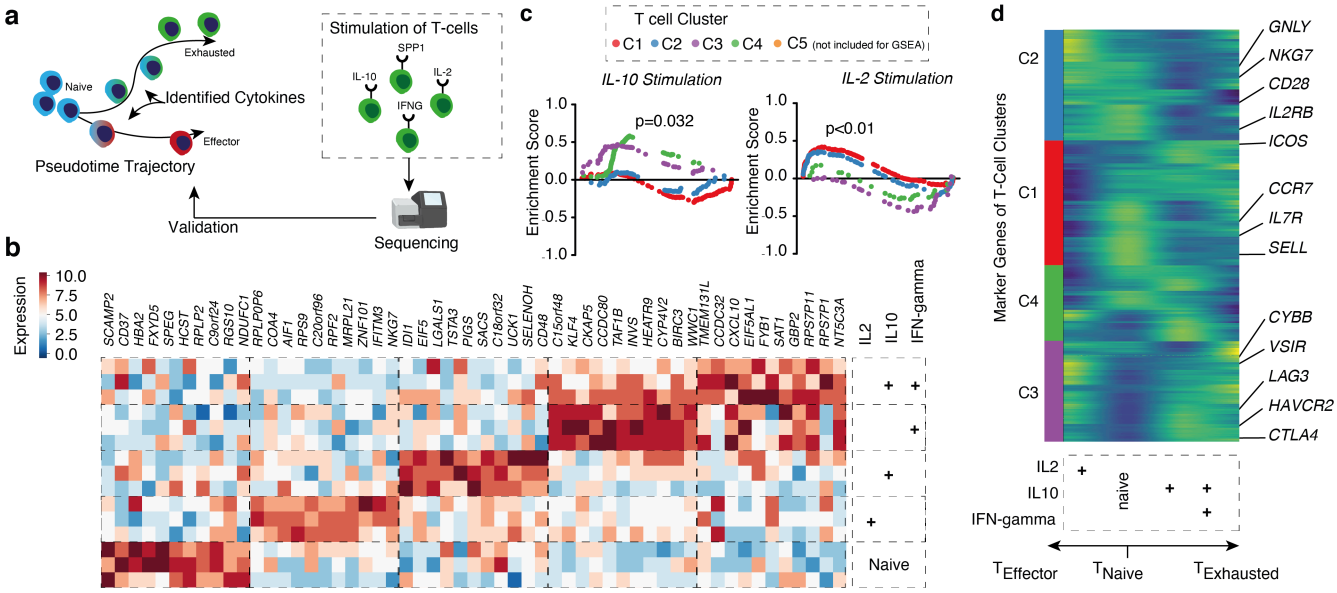

Figure 3

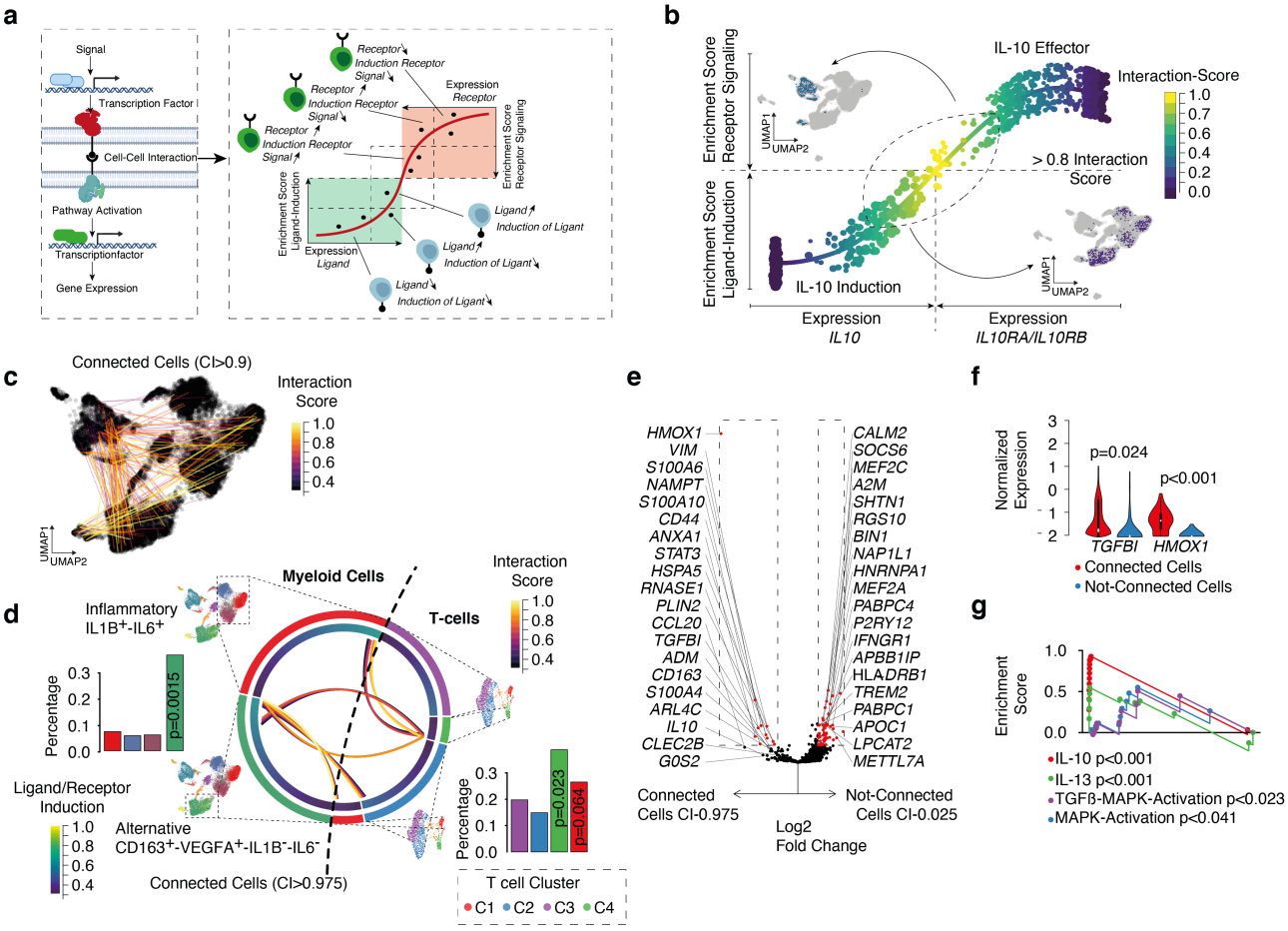

Figure 4

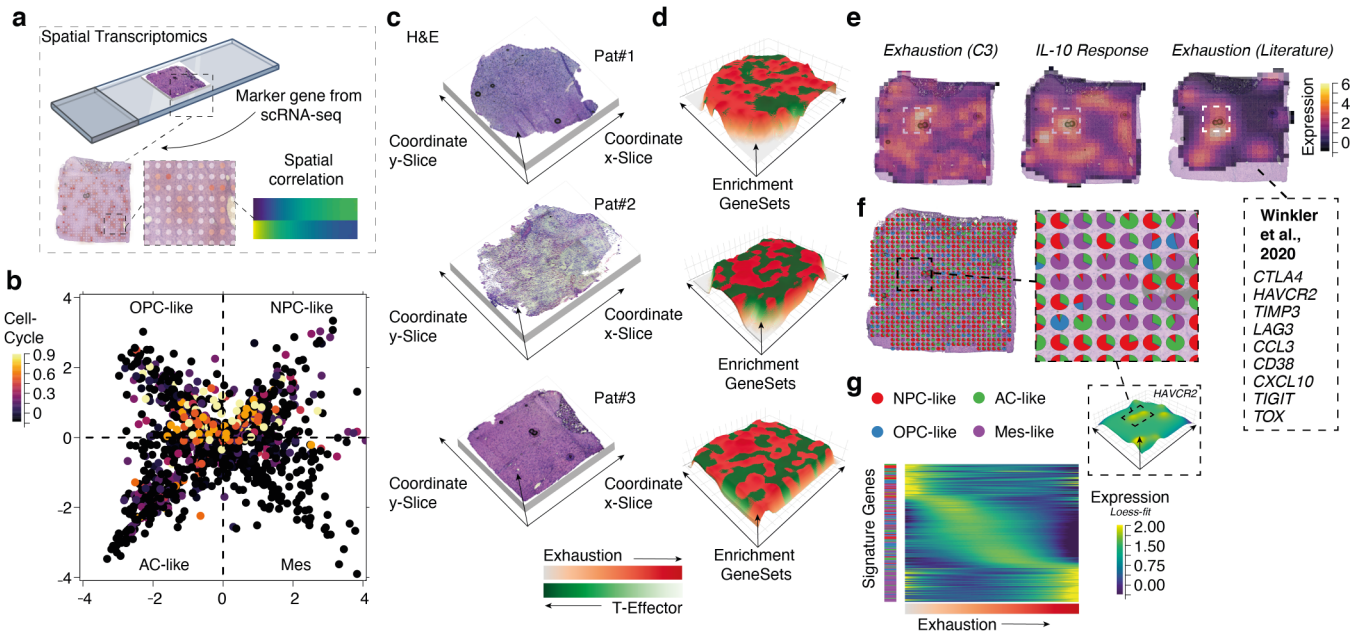

Figure 5

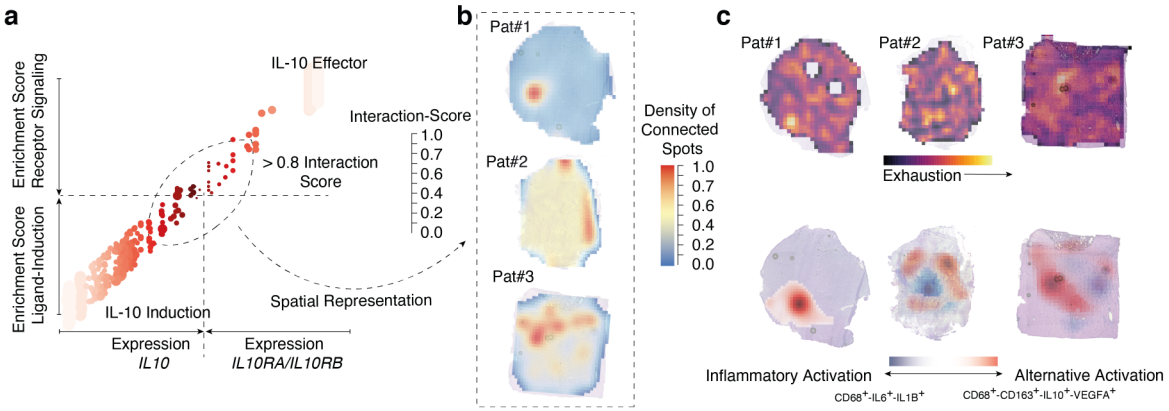

Figure 6

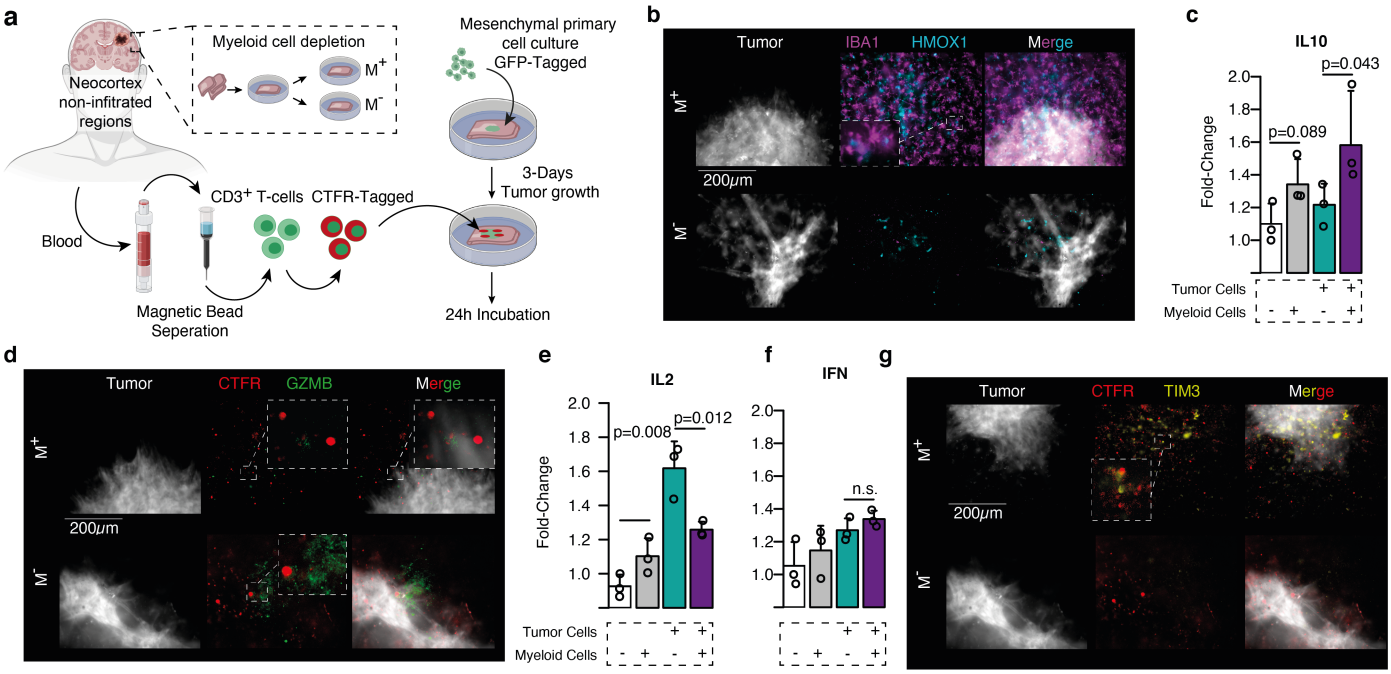

Supplementary Figure 1

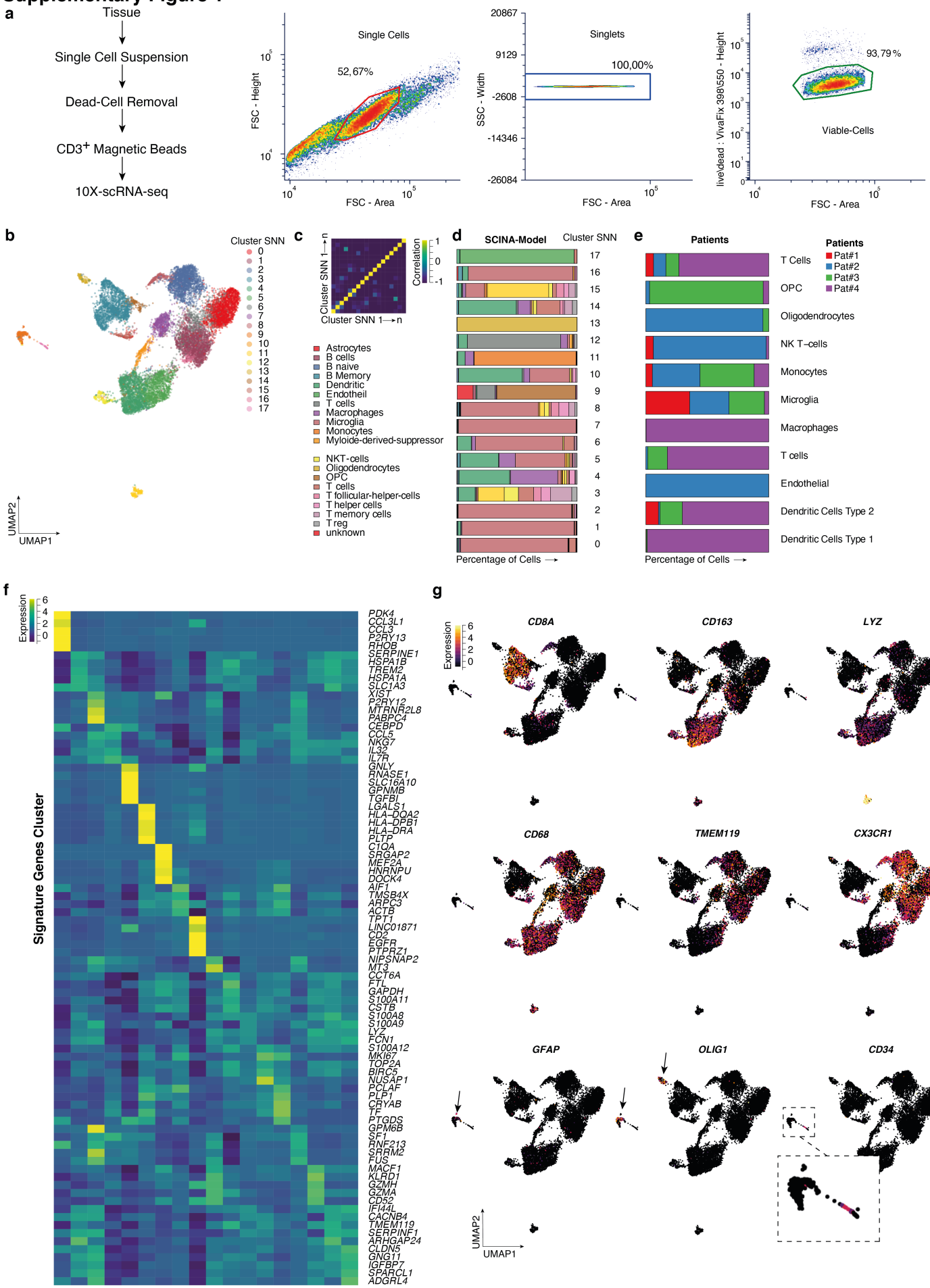

Supplementary Figure 2

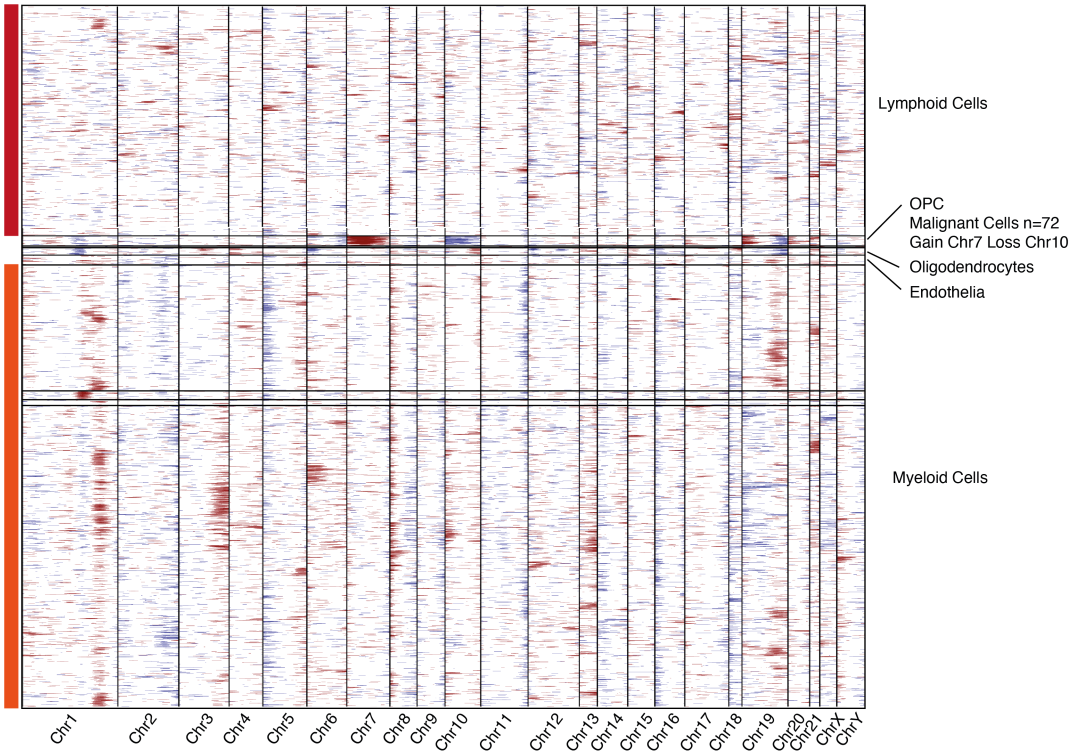

Supplementary Figure 3

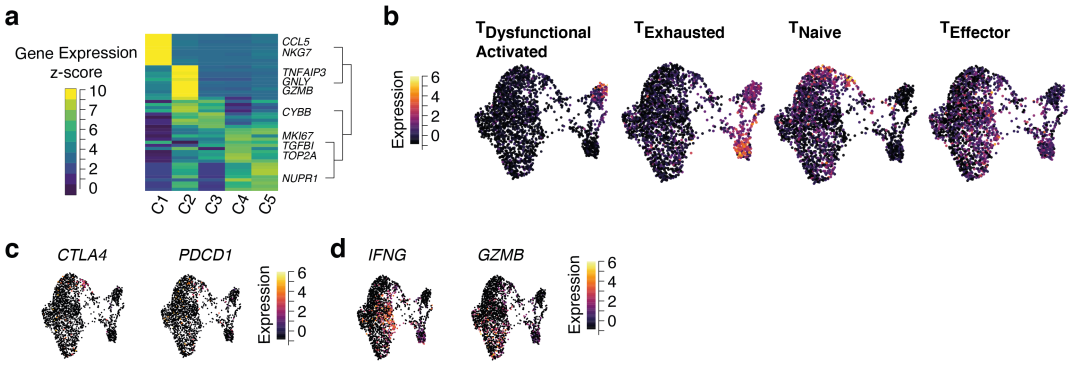

Supplementary Figure 4

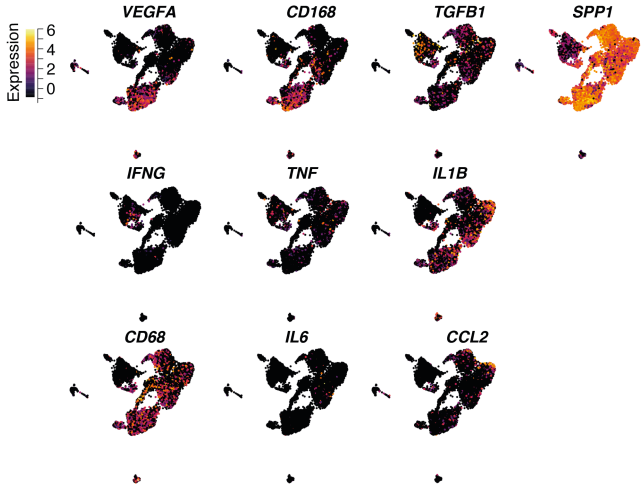

Supplementary Figure 5